Assessment of the Effectiveness of Conventional Rudder against Fish Tail and Tubercle Rudders at Various Angles of Attack

Sutiyo[1], Prima Ihda Kusuma Wardana[2], I Ketut Aria Pria Utama[2*]

[1] Department of Naval Architecture, Faculty of Engineering and Marine Sciences, Universitas Hang Tuah, Arief Rahman Hakim 150, Surabaya 60111, Indonesia

[2] Department of Naval Architecture, Faculty of Marine Technology, Institut Teknologi Sepuluh Nopember, Kampus ITS Sukolilo, Surabaya 60111, Indonesia, e-mail: kutama@its.ac.id

[*] Corresponding author

ARTICLE INFO

ABSTRACT

The development of maritime surface ships has become a significant topic in naval architecture due to the challenges posed by collisions and ship grounding. Special rudders, such as flaps and schilling rudders, are being developed to improve ship maneuverability and address carbon neutrality and environmental damage. Biomimicry, the study of replicating living/nature animals, aims to learn how to copy their systems, methods, forms, and structures, using them as eco-friendly and sustainable design solutions. Computational fluid dynamics (CFD) is increasingly being used in ship hydrodynamics to simulate complex phenomena in rudder simulations. The effectiveness of rudder use is determined by analysing the drag and side force values with various angles of attack from 0° to 30° at an operational speed of 12 knots. The most effective side force-to-drag ratio was achieved when the rudder was tilted at an angle of 5°. The fishtail and tubercle models have a more stochastic distribution, with the fishtail rudder having 5.1% greater performance effectiveness than the conventional rudder. The biomimetic method can improve the performance of wing-like structures, as seen with humpback whales operating in a marine environment similar to certain designed marine systems.

1 Introduction

Maritime transport is essential for the sustainability of global economic activity and industrial sectors [1]. According to the International Chamber of Shipping (ICS), the maritime transport sector carries about 90% of the goods generated by global commerce, with 80% of these goods being transported for the purpose of import and export [2]. Rudder optimisation is an important aspect of improving ship efficiency and reducing operational costs in global shipping, but it is only one of several approaches to achieve these goals. The optimisation of ship construction, including the rudder, hull, and propeller, is considered one of the two main approaches to reduce fuel consumption and optimise operational costs [3]. However, the context provided does not specifically focus on rudder optimisation as a primary method for improving global shipping efficiency. Many papers presented a more comprehensive view of ship efficiency optimisation, emphasising various strategies beyond rudder optimisation. The importance of ship speed optimisation, which has significant potential for improving energy efficiency according to the International Maritime Organization (IMO) [4], [5].

The ship's maneuvering characteristics encompass its turning, yaw-checking, course-keeping, and stopping abilities [6]. At the design stage, scale model tests and/or computer simulations can be conducted using mathematical models to accurately forecast the manoeuvrability of ships. It is necessary to carry out comprehensive maneuvering tests in order to confirm the accuracy of these findings [6]. The design stages of a commercial ship have traditionally paid little attention to maneuvering performance. As a result, certain ships have been constructed with inadequate maneuvering capabilities, leading to maritime accidents [7]. The resolution MSC.137(76) was adopted in December 2002 to estab-

lish uniform standards for ship maneuverability [8], ensuring that ships are designed accordingly. An effective rudder design is necessary for assisting good maneuvering [9].

Rudders are hydrofoils pivoting on a vertical axis, located at the stern behind propellers, to produce a transverse force and steering moment about the ship's center of gravity. To improve rudder effectiveness, factors such as rudder arrangement in the propeller stream, increased rudder area, better rudder, larger rudder angles in steering gear, and shorter rudder steering time can be considered [10]. However, extra investment in rudders can be costly for ship owners. The main problem is deciding whether to optimize rudder for service speed or low-speed maneuvering. Many rudder configurations can meet guidelines for turning circles and zig zag but may not be optimum for the ship's service profile. For some service profiles, good slow speed performance is crucial, and high rudder operating angles provide greater benefits [11], [12].

Naval architecture has closely focused on the development of maritime surface ship due to the serious problems caused by collisions and ship grounding. Special rudders, such as flaps and schilling rudders, are being developed to improve ship maneuverability[13]. In all engineering disciplines, computational techniques have become increasingly popular for design and optimisation applications. Complex phenomena can now be simulated using computational fluid dynamics (CFD) due to advances in computing power and parallel processing. Ship hydrodynamics increasingly incorporates CFD simulation techniques [14], [15]. Biomimicry implies striving to replicate living/nature animals. Biomimicry studies nature and living things to learn how to copy its systems, methods, forms, and structures. Imitate these qualities and use them as eco-friendly and sustainable design solutions to address challenges [16], [17], [18].

The present study proposes a CFD simulation approach for analysing three models of rudder models. Using computational fluid dynamics (CFD) methods, a case study was conducted to examine the conventional, fish tail, and tubercle rudder investigations of the General Cargo hull. In the context of three distinct rudder models, methodologies that are independent of grid resolution are employed, alongside specific boundary conditions and CFD simulation that reference ITTC standards [19], [20]. Subsequently, a comparable mesh, boundary criteria, and solving approaches were used to calculate the drag and side force at an operating speed of Vs = 12 knots using a similar mesh. The suggested ratio of the side force and drag at the design speed was determined to be ideal based on the findings obtained. This study sets a framework for applying CFD approaches to the effectiveness of the three rudder models.

2 Material and Method

2.1 Governing Equation

A three-dimensional CFD model employing a Reynolds-averaged Navier-Stokes (RANS) methodology has been developed to address flow-related challenges encountered in the hulls of ship. This approach facilitates the analysis of fluid motion and turbulence characteristics, enabling a comprehensive understanding of the hydrodynamic interactions that occur at the ship's surfaces [21], [22], [23]. The ANSYS-CFX program which was designed specifically for this purpose, employs a constant viscous incompressible flow equation. The two equations, averaged continuity, and momentum equations were used to express incompressible flows in this study [24]. The equations for mass and momentum are presented in Eqs. (1) and (2), respectively:

$$\frac{\partial \rho}{\partial t} + \nabla.(\rho U) = 0 \tag{1}$$

$$\frac{\partial(\rho U)}{\partial t} + \nabla.(\rho U \, x \, U) = -\nabla p + \nabla.\tau + S_M \tag{2}$$

where the stress tensor, τ is related to the strain rate.

The governing equation of total energy is presented in the Eq. (3):

$$\frac{\partial(\rho h_{tot})}{\partial t} - \frac{\partial p}{\partial t} + \nabla.(\rho U h_{tot}) =$$
$$= \nabla(\lambda \nabla T) + \nabla(U.\tau) + U.S_M + S_E \tag{3}$$

where h_{tot} is the total enthalpy.

The expression $+\nabla (U.\tau)$ accounts for the work resulting from viscous stresses and is referred to as the viscous work term. The term $U.S_M$ represents the work resulting from external momentum sources and is presently not taken into consideration.

Additionally, Reynolds-Averaged Navier-Stokes (RANS) was formulated as a modification of the steady Navier-Stokes's equations, incorporating both averaged and fluctuating variables. Anderson categorizes the turbulence model based on RANS equations as a statistical turbulence model because it relies on statistical averaging techniques in the derivation of the equations [25].

The **Menter's Shear Stress Transport** (popularly known as SST) turbulence model effectively formulates a versatile approach for various applications by integrating the advantages of the k-ω model with other relevant factors[26], [27]. The k–omega (k–ω) turbulence model, a prevalent two-equation turbulence model, approximates the Reynolds-averaged Navier–Stokes (RANS) equations. It predicts turbulence using two partial differential equa-

(a) MV. SERENITY 09 at sea going

(b) MV. SERENITY 09 Lines with Rudder

Figure 1 MV SERENITY 09

tions for variables k (turbulence kinetic energy) and ω (specific rate of dissipation of k into internal thermal energy). To achieve this, it incorporates a blending function called F1, which takes a value of one in the region immediately adjacent to the solid surface and gradually decreases to zero as one moves further away from the wall into the flow domain. This arrangement activates the k-ω model near the wall and employs the k-ε model for the rest of the flow. The k-epsilon (k-ε) turbulence model enhances the mixing-length model and offers an alternative for algebraically determined turbulent length scales in moderate to complex flows, focusing on the turbulent kinetic energy (k) and its dissipation rate (ε). This approach enables the beneficial near-wall characteristics of the k-ω model to be utilized without the risk of introducing inaccuracies stemming from the model's sensitivity to free stream conditions. The modelled equations for turbulent kinetic energy (k) and turbulence frequency (ω) are shown in Eqs. (4) and (5).

$$\frac{\partial(\rho k)}{\partial t} + \frac{\partial(\partial u_j k)}{\partial x_j} =$$

$$= P - \beta^* \rho \omega k + \frac{\partial}{\partial x_j}\left[(\mu + \sigma_k \mu_t)\frac{\partial k}{\partial x_j}\right] \quad (4)$$

$$\frac{\partial(\rho\omega)}{\partial t} + \frac{\partial(\rho u_j\omega)}{\partial x_j} = \frac{\gamma}{v_t}P - \beta\rho\omega^2 + $$

$$+ \frac{\partial}{\partial x_j}\left[(\mu + \sigma_\omega \mu_t)\frac{\partial\omega}{\partial x_j}\right] + 2(1 - F_1)2\rho\sigma_{\omega 2}\frac{1}{\omega}\frac{\partial k}{\partial x_j}\frac{\partial\omega}{\partial x_j} \quad (5)$$

Table 1 Particular Dimension

Parameter	Symbol	Unit	Value
Length Over All	LOA	m	92.70
Length of Perpendicular	LBP	m	83.96
Breadth Moulded	Bmld	m	15.10
Depth Moulded	Dmld	m	7.70
Draft	T	m	4.60
Displacement	Δ	ton	4384

2.2 Geometry

The focus of the conducted study was the rudder of a general cargo ship named MV. Serenity, identified by its IMO number 8820949 [28], as seen in Figure 1. The details of the rudder can be found in Table 1. The present operation of this vessel is the transportation of commodities to the eastern area of Indonesia.

Conventional rudder size in accordance with Indonesian ship classification (BKI) requirements [29] is considered and the NACA 0018 airfoil is used. These restrictions are then amended to the rudder width by taking into consideration the fact that the rudder height value has not altered. The design process for the rudder began with the establishment of a standard rudder configuration that adhered to the regulations set forth by the Indonesian ship classification authority (BKI), as depicted in Figure 2(a). Following this initial design, modifications were made to introduce a fish tail configuration, illustrated in
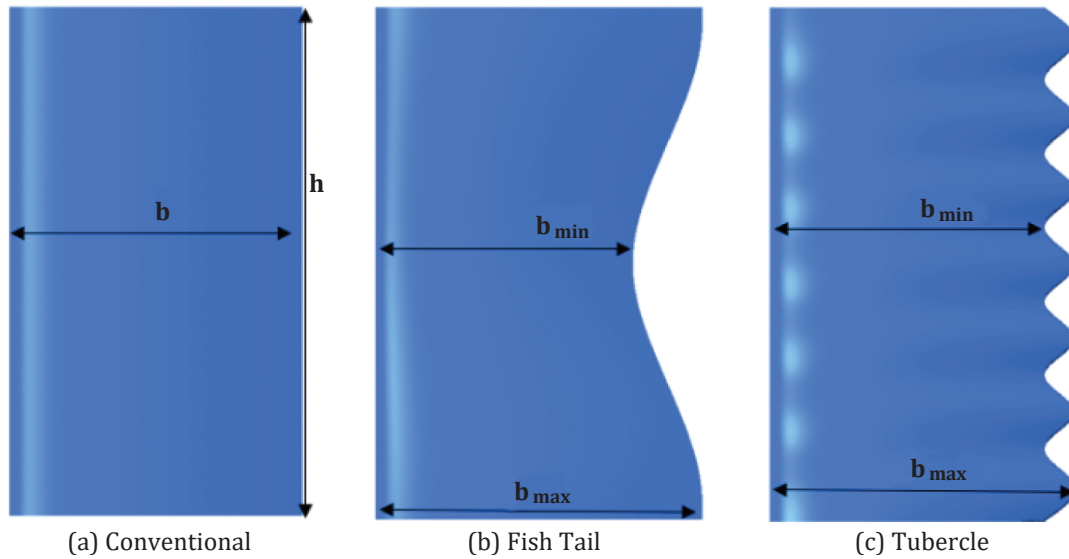
(a) Conventional   (b) Fish Tail   (c) Tubercle

Figure 2 Rudder Variations

Table 2 Specifications of Rudder Dimension

Dimension	Unit	Rudder Type		
		Conventional	Fish Tail	Tubercle
Height (h)	m	2.33	2.33	2.33
Breadth (b)	m	1.27	-	-
Breadth minimum (bmin)	m	-	1.11	1.19
Breadth maximum (bmax)	m	-	1.40	1.33
Area of rudder surface (A)	m^2	6.2	6.2	6.2

Figure 2(b), and further alterations were applied to create a tubercle shape that draws inspiration from the anatomy of whales, as represented in Figure 2(c). This research utilized the biomimetic characteristics of fish, which are known for their effective propulsion in aquatic environments. A hydrodynamic analysis was performed based on an equivalent rudder area, detailed in Table 2.
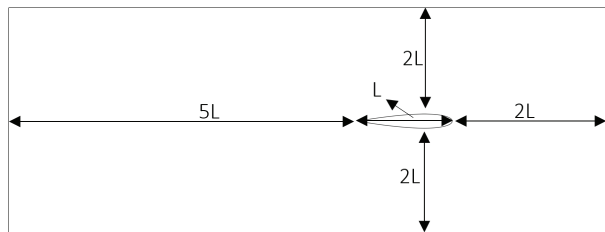
2.3 Numerical Domain

The suggested computational domain of boundary condition as shown Figure 3(a) with 2L forward, perpendicular to the front, at the velocity intake, and 5L towards the rear, perpendicular to the outlet pressure. Both of these directions extend in the same direction. Through the implementation of the transverse and vertical directions to 2L-3L [30], [31], [32], we were able to avoid the adverse effects of reverse flow on the boundaries of the region. Figure 3(b) depicts the boundary conditions as well as the size of the domain The water is moving out of the region at a speed of 12 knots, which is the definition of outlet flow. The inlet flow velocity is 12 knots. it is shown that the hull body is considered to be a fixed boundary, and the walls are given a symmetry constraint.
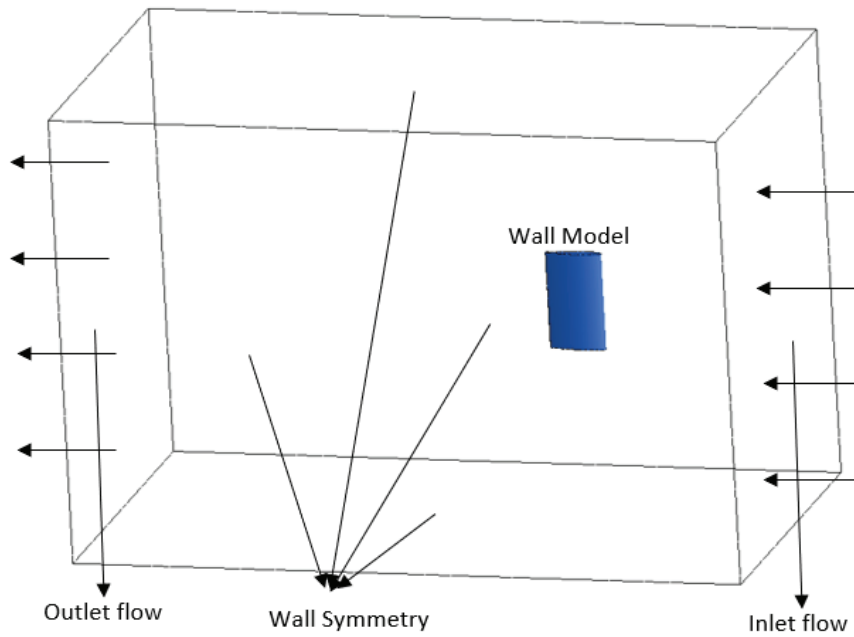
(a) Boundary Condition
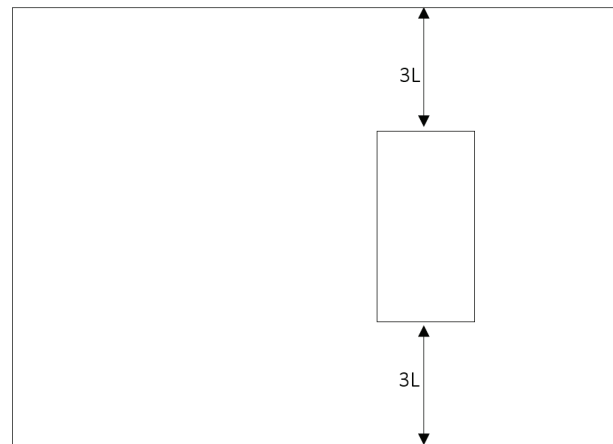
(i) top view   (ii) side view

(b) model to domain distance

Figure 3 Numerical Domain

2.4 Meshing and Grid Independence

The use of Design Modeler was required to complete the process of mesh construction for this investigation. A combination of structured and unstructured meshes are used in order to discretize the computation domain. In consideration of the intricate geometrical features of the hull, a mesh consisting of triangle elements is constructed on the surface of the hull. Subsequently, the boundary layer is refined using prism elements that are generated by expanding the surface mesh node. Inflated tetrahedral elements are used to populate the area close to the boat, while an unstructured mesh with grid gen-

eration is used to reduce the total number of components in the distant field (as illustrated in Figure 4).

However, it is likely that fine mesh will always offer credible outcomes for ANSYS CFX, the fact that it contains a high number of components will also result in an increase in the amount of time and resources that is needed for computation. A significant consideration to take into account throughout the computing process is the size of the mesh. Mesh convergence is carried out on both the subsurface model, as demonstrated in Figure 5. The overall mesh count of around 1.6 million has been achieved in the case of rudders, which indicates that the
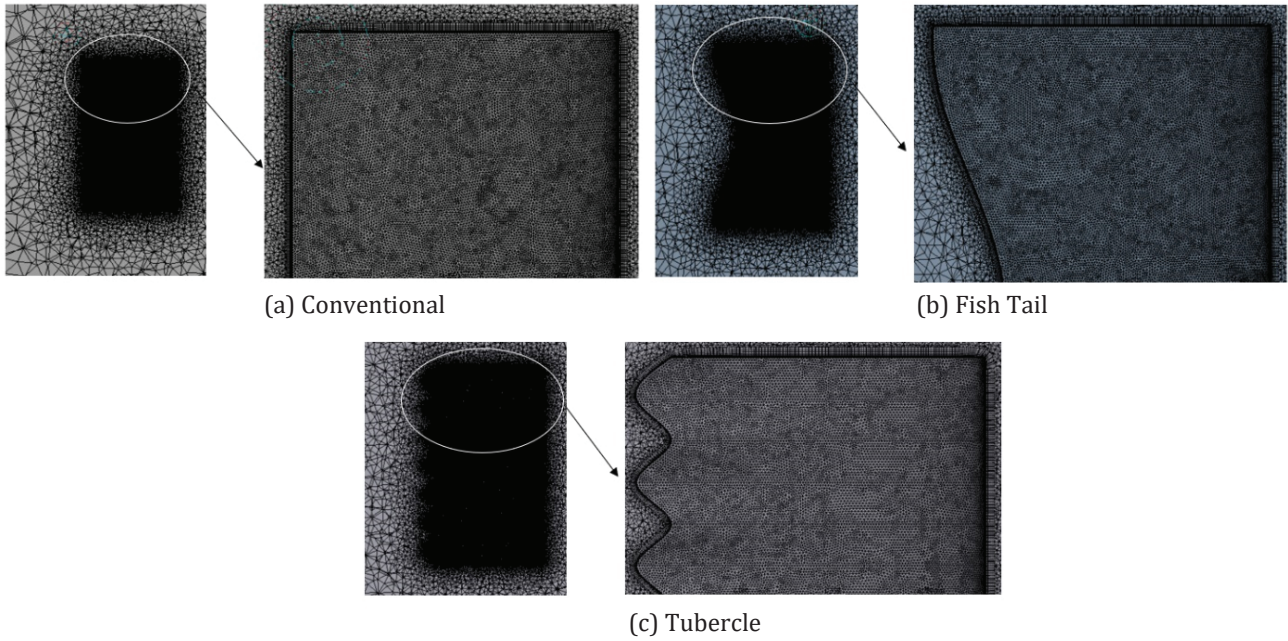
(a) Conventional

(b) Fish Tail

(c) Tubercle

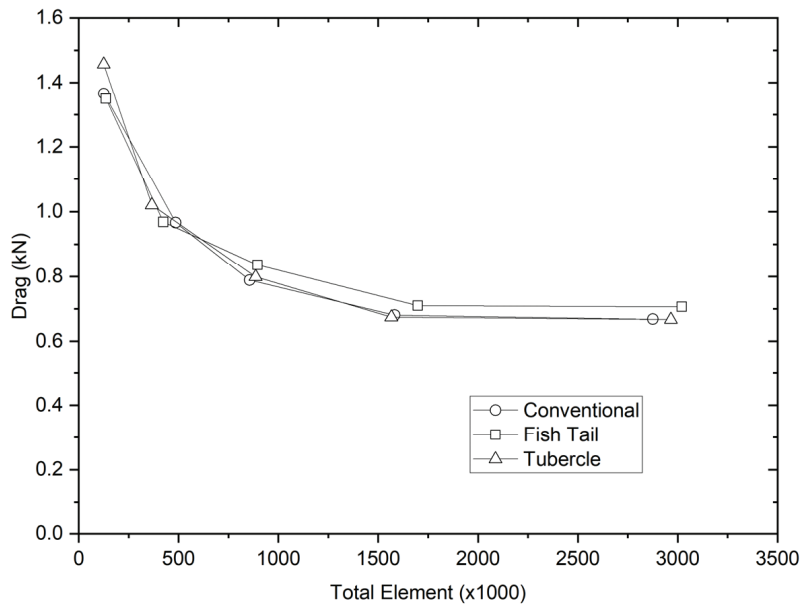**Figure 4** Hybrid Mesh at various rudder

Figure 5 Grid Independence Study

optimal mesh convergence has been achieved. Anderson's findings, which show that there is a difference in the total drag coefficient that is less than 2%, offer confidence to the impression that this convergence is really occurring [25].

3 Results and Discussion

The effectiveness of rudder use is determined by analysing the drag and side force values associated with the rudder. Figure 6 displays the computed values for drag and side force. This table explains that the rudder's drag and side force values are affected by the configuration created by the rudder in the direction of the flow. According to this data, there is a direct correlation between the magnitude of the angle created and the values of drag and side force, indicating that as the angle increases, so do the drag and side force values.

The conventional rudder shape, with modifications to the fish tail and tubercles, exhibits nearly the same
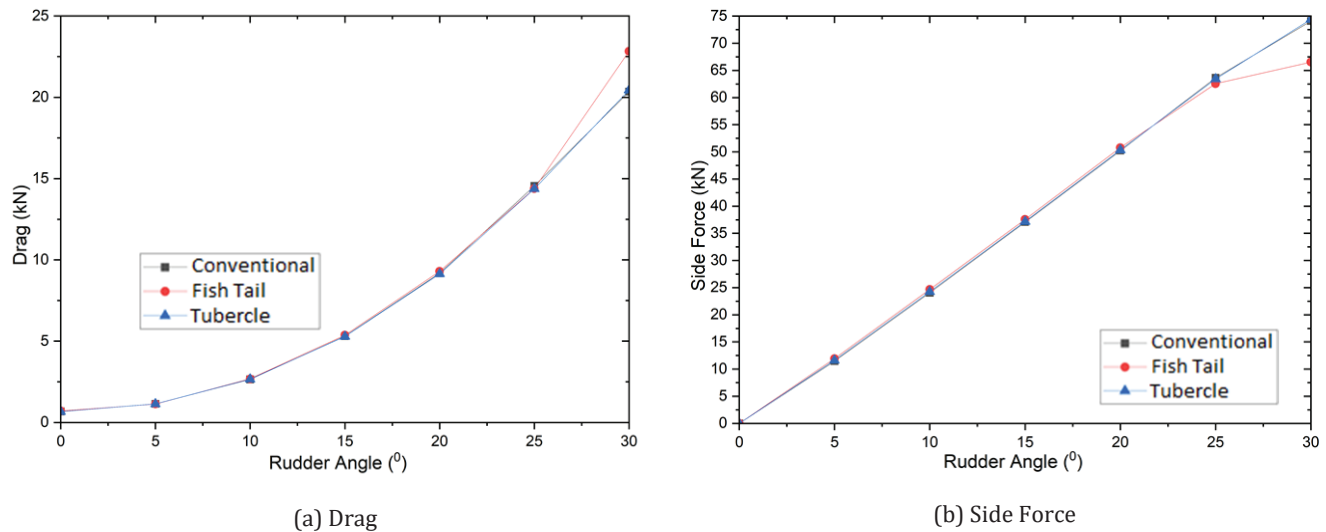
(a) Drag   (b) Side Force

Figure 6 CFD Calculation of Rudder Variation

drag value, differing by an average of 2.6% compared to the fish tail and 0.2% compared to the tubercles shape. There is a notable disparity in the shape of the fish tail when the rudder is angled at 30 degrees, resulting in a 12.2% increase compared to the conventional shape (Figure 6(a)).

Furthermore, there is a more significant difference in the values of the side force. There is a reduction in side force at an angle of 30 degrees, as indicated in Figure 6(b), and the fish tail side force has an average difference that is 2.8% higher than the conventional shape. Figure 6 demonstrates this; as indicated in Figure 6(b), the difference in side force is 0.68% higher in the tubercle shape than it is in the traditional shape. This is the case when comparing the two shapes.

It is possible to describe the factors that contribute to variations in the values of the rudder's drag and side force by employing CFD simulations in conjunction with the appropriate methodological approaches. In general, variations in the shape of the rudder have a significant impact on the values of drag and side force, despite the fact that they include virtually the same amount of surface (Table 3). The size of the interaction between the water and the model, which takes the form of pressure on it, has an effect on the magnitude of the values of the side force and the drag. In order to provide a critical and representative depiction of the rudder that is being analysed, the features are provided at angles of 5 and 30 degrees. This is fairly obvious, as seen in Figures 7 and 8.

There is a considerable relationship between the amount of pressure that is applied to the rudder region and the quantity of drag that is produced. A visualization of the distribution of pressure and side force on the three different rudder models is presented in Figure 7, which may be found to the right. The visualization that can be explained in this figure is that the pressure dis-

tribution on the rudder tubercle (Figure 7(c)) has the greatest red area (high pressure) in comparison to other models. This is the case since the red area covers the highest pressure. Following the traditional rudder comes the rudder with a fish fin shape, which is the smallest of the three different types of rudders. This gives a clear picture that the drag value is in accordance with Table 4, which is a very satisfactory result.

Following that, an upward arrow is displayed at the side force value, which represents a sideways force (which is perpendicular to the direction in which the water is flowing). This indicates that the direction of the arrow is perpendicular to the flow. In the meantime, the colour of the arrow indicates the magnitude of the value of the side force. The distribution of side forces and the direction in which they are acting are both depicted in this visualisation in great detail. The standard rudder model has a side force distribution that is distributed in a regular manner, but the tail fish and tubercle models have a side force distribution direction that is more random. The value of each side force in the model, on the other hand, is relatively the same. This is demonstrated by an accurate figure of total side force coming in at 11.48 kN for the conventional rudder, 11.93 kN for the fish tail rudder, and 11.62 kN for the tubercle rudder. When compared to the other models, the fish model offers the greatest amount of secondary force. When the angle of the fishtail rudder is set to five degrees, this condition has a beneficial impact on the navigation of the vessel.

The most effective ratio of side force to drag is achieved when the rudder is tilted at an angle of 5 degrees. The conventional rudders have a value of 10.03, the fish tail rudders and tubercle rudders have a value of 10.54 and 10.13, respectively. These numbers quantify the degree of efficacy of lateral force on rudder resist-
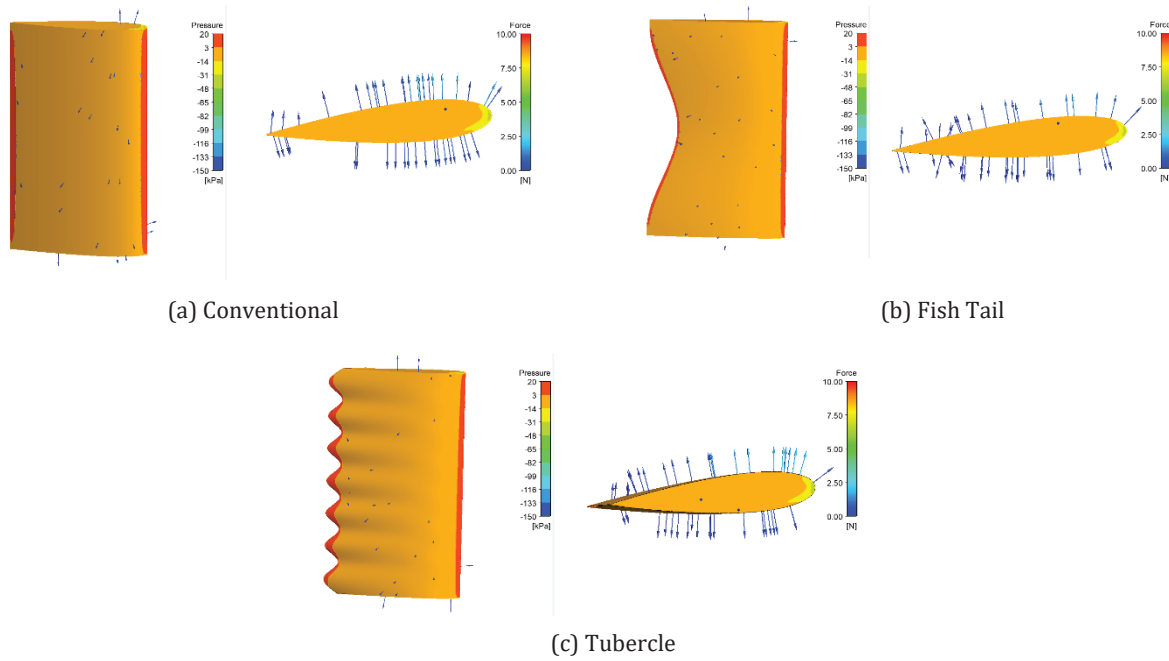
(a) Conventional   (b) Fish Tail

(c) Tubercle

Figure 7 Pressure and Side Fore Distribution at 5^0

ance. The rudder efficacy improves as the ratio value increases. Therefore, the rudder designed with a fish tail shape exhibits a performance effectiveness that is 5.1% more than the conventional shape, whilst the rudder with the tubercle shape demonstrates a performance effectiveness that is 1% higher than conventional rudder.

Nevertheless, the rudder's performance declines as the angle reaches 25 degrees and exhibits a much worse performance at 30 degrees, with a drop of 19.97% compared to the traditional design. Conversely, the rudder with a tubercle shape has best performance at all angles, except at 0 and 30 degrees. The research conducted by Weber et al. [33] is highly relevant, demonstrating a decrease in lift force at approximately 15 degrees. For further details, see Figure 8.

The effectiveness of the rudder, which has a fish tail shape and is inclined at an angle of 5 degrees, is clearly seen in Figure 9(b), where the flow is uniformly distributed on both sides of the rudder. This enhances the
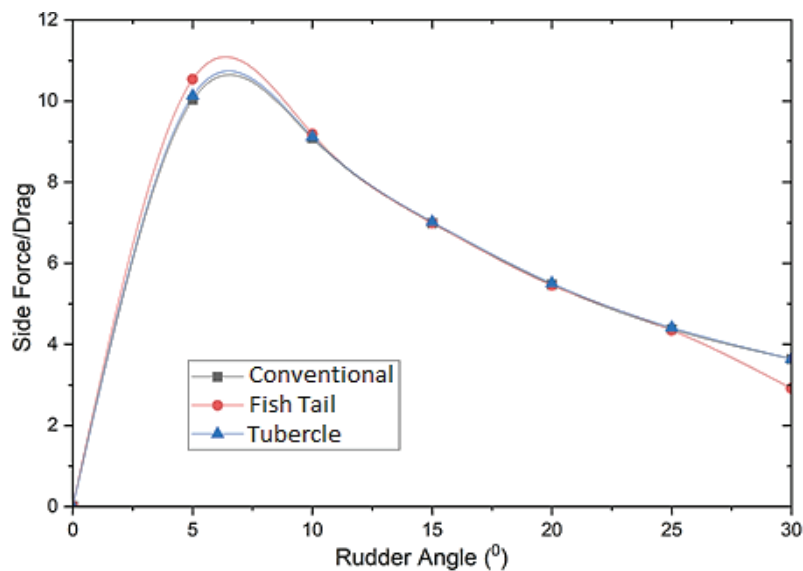

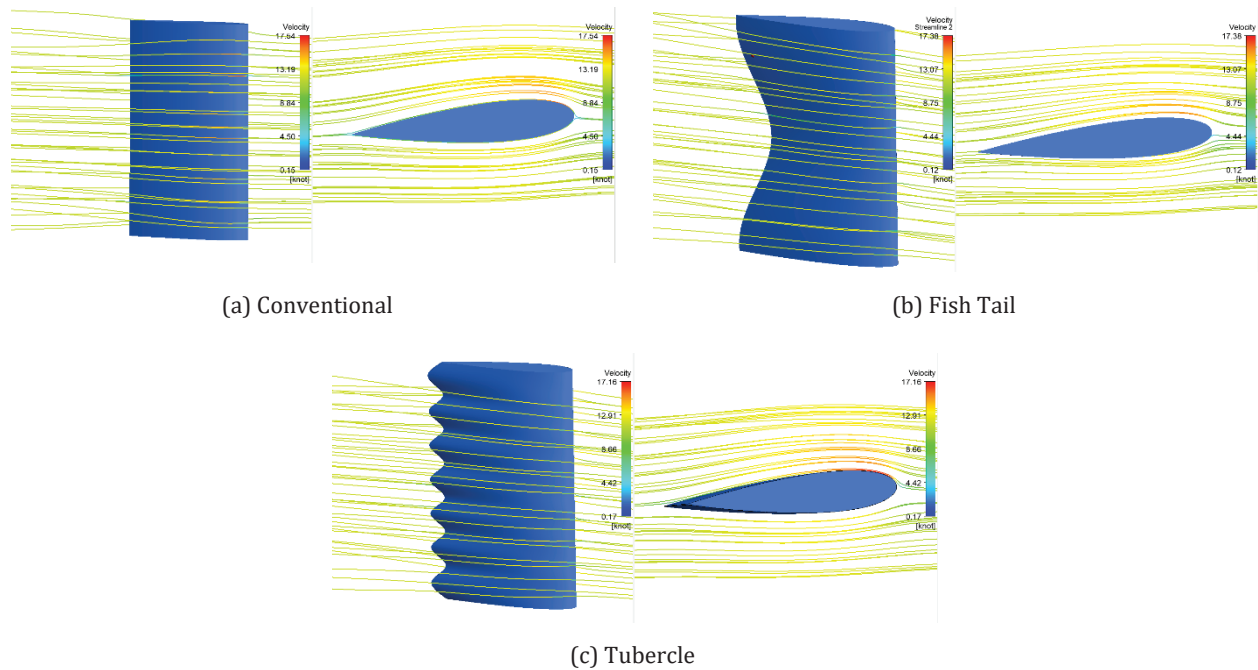**Figure 8** CFD Calculation of Side Force/Drag at Rudder Variation

(a) Conventional

(b) Fish Tail

(c) Tubercle

Figure 9 Fluid flow over the rudder at 5^0

magnitude of the lateral force, hence improving the ratio of lateral force to drag, which in turn improves the efficiency of the rudder's performance. The airflow from the front will be directed into a cavity located in the centre of the fish tail rudder and then evenly dispersed around the surface of the rudder. Meanwhile, both conventional and tubercle-shaped rudders have a similar propensity for the flow to be evenly distributed, indicating that there is no optimisation of the rudder form, as seen in Figures 9(a) and 9(c).

Technology is advanced via the biomimetic method, which involves the transfer of technology from natural technologies to artificially systems. Particularly compared to the post-stall situation of conventional wings, the hydrodynamic effect has the ability to postpone stalling to greater angles of attack, enhance lift, and minimize drag. The usage of tubercles has the potential to improve the performance of wing-like structures. This is because the humpback whale operates in the marine environment in a Reynolds number regime that is comparable to that of certain designed marine systems [17]. This is followed by the imitation and implementation of these features as suitable architectural solutions in order to address issues in a way that is both environmentally friendly and sustainable [18].

4 Conclusion

The simulation limitations are solely based on studies utilising CFD at the same flow velocity and employing only the SST Turbulence model. The effectiveness of

rudder use was determined by analyzing the drag and side force values. The configuration created by the rudder in the flow direction affected these values. A direct correlation exists between the magnitude of the created angle and the values of the drag and side forces. The conventional rudder model has a prescribed side-force distribution, whereas the fishtail and tubercle models have a more stochastic distribution. The fish model generated the least side force, but operating the fishtail rudder at 30° was affected. The most effective side force-to-drag ratio was achieved when the rudder was tilted at an angle of 5°. The fishtail rudder has 5.1% more performance effectiveness than the conventional rudder, whereas the tubercle rudder has 1% superior performance. However, the rudder performance declines as the angle reaches 25° and 30°, with a drop of 19.97% compared to the traditional design. The use of biomimetic techniques can improve efficiency in a maritime environment, comparable to that of specific engineered marine systems. This innovative approach to rudder design demonstrates the potential of biomimetic principles to enhance maritime technology, although further research is required to optimize performance across all operational angles in correlation with ship manoeuvring performance.

References

[1] J. M. Lane and M. Pretes, "Maritime dependency and economic prosperity: Why access to oceanic trade matters," *Mar Policy*, vol. 121, p. 104180, Nov. 2020, doi: 10.1016/J.MARPOL.2020.104180.

[2] "Shipping and World Trade: World Seaborne Trade | International Chamber of Shipping." Accessed: Dec. 28, 2023. [Online]. Available: https://www.ics-shipping.org/shipping-fact/shipping-and-world-trade-world-seaborne-trade/

[3] Y. Sharifi, H. Ghassemi, and H. Zanganeh, "Various Innovative Technologic Devices in Shipping Energy Saving and Diminish Fuel Consumption," *International Journal of Physics, Vol. 5, 2017, Pages 21-29*, vol. 5, no. 1, pp. 21–29, Feb. 2017, doi: 10.12691/IJP-5-1-4.

[4] X. Li, Y. Gu, X. Fan, K. Zou, and X. Hou, "An Optimization Model for Ship Speed Based on Maneuvering Control," *J Mar Sci Eng*, vol. 11, no. 1, p. 49, Dec. 2022, doi: 10.3390/jmse11010049.

[5] Y. Sang, Y. Ding, J. Xu, and C. Sui, "Ship voyage optimization based on fuel consumption under various operational conditions," *Fuel*, vol. 352, p. 129086, Nov. 2023, doi: 10.1016/j.fuel.2023.129086.

[6] H. Yasukawa and Y. Yoshimura, "Introduction of MMG standard method for ship maneuvering predictions," *Journal of Marine Science and Technology (Japan)*, vol. 20, no. 1, pp. 37–52, Mar. 2015, doi: 10.1007/S00773-014-0293-Y.

[7] Y. Guo, Y. Jin, S. Hu, Z. Yang, Y. Xi, and B. Han, "Risk evolution analysis of ship pilotage operation by an integrated model of FRAM and DBN," *Reliab Eng Syst Saf*, vol. 229, p. 108850, Jan. 2023, doi: 10.1016/J.RESS.2022.108850.

[8] I. Maritime Organization, "RESOLUTION MSC.137(76) (adopted on 4 December 2002) STANDARDS FOR SHIP MANOEUVRABILITY," 2002.

[9] A. H. Muhammad, D. Paroka, S. Rahman, and M. R. Firmansyah, "Twin-Rudder-System Configurations' Impact on Ferry Ships' Course-Keeping Ability under Windy Conditions," *International Journal of Technology*, vol. 12, no. 2, pp. 432–443, 2021, doi: 10.14716/IJTECH.V12I2.3829.

[10] Y.-J. ; Shin *et al.*, "Maneuverability Performance of a KRISO Container Ship (KCS) with a Bulb-Type Wavy Twisted Rudder and Asymmetric Pre-Swirl Stator," *Journal of Marine Science and Engineering 2023, Vol. 11, Page 2011*, vol. 11, no. 10, p. 2011, Oct. 2023, doi: 10.3390/JMSE11102011.

[11] M. Ueno, R. Suzuki, and Y. Tsukada, "Full-scale ship propeller torque in wind and waves estimated by free-running model test," *Ocean Engineering*, vol. 184, pp. 332–343, Jul. 2019, doi: 10.1016/j.oceaneng.2019.04.057.

[12] R. Suzuki, Y. Tsukada, and M. Ueno, "Estimation of full-scale ship manoeuvrability in adverse weather using free-running model test," *Ocean Engineering*, vol. 213, Oct. 2020, doi: 10.1016/j.oceaneng.2020.107562.

[13] S. Li, T. Wang, G. Li, and H. Zhang, "Ship maneuvering model optimization for improved identification with less excitation," *Ocean Engineering*, vol. 280, p. 114540, Jul. 2023, doi: 10.1016/J.OCEANENG.2023.114540.

[14] R. Broglia *et al.*, "Assessment of Computational Fluid Dynamics Capabilities for the Prediction of Three-Dimensional Separated Flows: The Delft 372 Catamaran in Static Drift Conditions," *Journal of Fluids Engineering, Transactions of the ASME*, 2019, doi: 10.1115/1.4042752.

[15] Sutiyo and I. K. A. P. Utama, "CFD Analysis into the Drag Characteristics of Trimaran Vessel: Comparative Study between Standard NPL 4a and the use of Axe-Bow," *IOP Conf Ser Earth Environ Sci*, vol. 799, no. 1, p. 12007, Jun. 2021, doi: 10.1088/1755-1315/799/1/012007.

[16] A. Ramezani, S. J. Chung, and S. Hutchinson, "A biomimetic robotic platform to study flight specializations of bats," *Sci Robot*, vol. 2, no. 3, Feb. 2017, doi: 10.1126/SCIROBOTICS.AAL2505.

[17] F. E. Fish, P. W. Weber, M. M. Murray, and L. E. Howle, "Marine applications of the biomimetic humpback whale flipper," *Mar Technol Soc J*, vol. 45, no. 4, pp. 198–207, Jul. 2011, doi: 10.4031/MTSJ.45.4.1.

[18] F. E. Fish, P. W. Weber, M. M. Murray, and L. E. Howle, "The tubercles on humpback whales' flippers: Application of bio-inspired technology," *Integr Comp Biol*, vol. 51, no. 1, pp. 203–213, Jul. 2011, doi: 10.1093/ICB/ICR016.

[19] ITTC, "ITTC-Recommended Procedures and Guidelines: Practical Guidelines for Ship CFD Applications," 2011.

[20] ITTC, "ITTC-Recommended Procedures and Guidelines Uncertainty Analysis in CFD Verification and Validation Methodology and Procedures," 2017.

[21] A. Miao, M. Zhao, and D. Wan, "CFD-based multi-objective optimisation of S60 Catamaran considering Demihull shape and separation," *Applied Ocean Research*, 2020, doi: 10.1016/j.apor.2020.102071.

[22] I. K. A. P. Utama, A. Jamaluddin, and Sutiyo, "Development of Free-Surface CFD Modelling into The Breakdown of Ship Resistance Components," in *12th International Conference on QiR (Quality in Research)*, Bali, July. 2011, pp. 1064–1070.

[23] I. K. A. P. Utama, Sutiyo, I. K. Suastika, A. Sulisetyono, Y. A. Hermawan, and W. D. Aryawan, "Resistance Analysis of Rescue Boat in Calm Water Condition," *IOP Conf Ser Mater Sci Eng*, vol. 1052, no. 1, p. 012062, Jan. 2021, doi: 10.1088/1757-899X/1052/1/012062.

[24] ANSYS, *ANSYS CFX-Solver Theory Guide*. Canonsburg, PA, USA: Ansys Inc, 2020.

[25] J. D. Anderson, *Computational Fluid Dynamics: The Basics with Applications*. in Editions: Mechanical Engineering. New York, USA. pp. 526-532: McGraw-Hill, 1995.

[26] F. R. Menter, "Zonal two equation κ-ω turbulence models for aerodynamic flows," in *AIAA 23rd Fluid Dynamics, Plasmadynamics, and Lasers Conference, 1993*, 1993, pp. 1–21.

[27] F. R. Menter, M. Kuntz, and R. Langtry, "Ten Years of Industrial Experience with the SST Turbulence Model," in *4th Internal Symposium, Turbulence, heat and mass transfer*, New York, Wallingford: Begell House, 2003, pp. 625–632.

[28] BKI, "MV. SERENITY - 09." Accessed: Dec. 29, 2023. [Online]. Available: https://www.bki.co.id/shipregister-22338.html

[29] BKI, "Rules for Classification and Construction Part 1 Seagoing Ships RULES FOR HULL Volume II 2024 Consolidated," 2024.

[30] A. G. Elkafas, M. M. Elgohary, and A. E. Zeid, "Numerical study on the hydrodynamic drag force of a container ship model," *Alexandria Engineering Journal*, vol. 58, no. 3, pp. 849–859, Sep. 2019, doi: 10.1016/j.aej.2019.07.004.

[31] Y. min Su, J. feng Lin, D. gang Zhao, C. yu Guo, and H. Guo, "Influence of a pre-swirl stator and rudder bulb system on the propulsion performance of a large-scale ship model," *Ocean Engineering*, vol. 218, Dec. 2020, doi: 10.1016/J.OCEANENG.2020.108189.

[32] I. K. A. P. Utama, W. D. Aryawan, A. Nasirudin, Sutiyo, and Yanuar, "Numerical Investigation into the Pressure and Flow Velocity Distributions of a Slender-Body Catamaran Due to Viscous Interference Effects," *International Journal of Technology*, vol. 12, no. 1, p. 149, Jan. 2021, doi: 10.14716/ijtech.v12i1.4269.

[33] P. W. Weber, L. E. Howle, and M. M. Murray, "Lift, Drag, and Cavitation Onset on Rudders With Leading-Edge Tubercles," *Mar. Technol.*, vol. 47, no. 1, pp. 27–36, Jan. 2010.